ACADEMIC PRESS

Available online at www.sciencedirect.com
SCIENCE DIRECT®

Journal of Solid State Chemistry 173 (2003) 407–417

JOURNAL OF SOLID STATE CHEMISTRY

http://elsevier.com/locate/jssc

Structural investigation of $R_2Mo_4O_{15}$ (R = La, Nd, Sm), and polymorphs of the $R_2Mo_4O_{15}$ (R = rare earth) family

H. Naruke* and T. Yamase

Chemical Resources Laboratory, Tokyo Institute of Technology, 4259 Nagatuta, Midori-ku, Yokohama 226-8503, Japan

Received 2 October 2002; received in revised form 31 January 2003; accepted 20 February 2003

Abstract

Pyrolysis of rare earth (R) polyoxomolybdate, $[R_2(H_2O)_{12}Mo_8O_{27}]\cdot xH_2O$ (R = La, Nd and Sm), at 750°C for 2–8 h results in crystallization of $R_2Mo_4O_{15}$ compounds. β-$La_2Mo_4O_{15}$ crystallizes together with an α-form in monoclinic $P2_1/a$ (No. 14), $a = 13.8893(5)$, $b = 13.0757(4)$, $c = 20.0927(8)$ Å, $\beta = 95.199(2)°$, $V = 3634.1(2)$ Å^3, $Z = 12$, $R_1(I > 2\sigma(I)) = 0.048$, R_w (all data) = 0.116. The structure is built up with $\{LaO_n\}$ ($n = 9$, 10) and $\{MoO_{n'}\}$ ($n' = 4-6$) polyhedral units. The $\{LaO_n\}$ units are polymerized into a linear $\{La_6O_{39}\}_\infty$ chain, while the $\{MoO_n\}$ are connected together to form $\{Mo_4O_{15}\}$ and $\{Mo_7O_{26}\}$ groups. The structure can be related to the α-form by partial rearrangement of O atoms and small shifts of La and Mo atoms. The $R_2Mo_4O_{15}$ (R = Nd and Sm) compounds are isomorphous with the previously reported R = Eu and Gd analogs, crystallizing in triclinic, $P\bar{1}$ (No. 2), $a = 9.4989(5)$ and 9.4076(7), $b = 11.0088(7)$ and 10.9583(8), $c = 11.5665(6)$ and 11.5234(8) Å, $\alpha = 104.141(3)$ and 104.225(3), $\beta = 109.838(3)$ and 109.603(3), $\gamma = 108.912(3)$ and 108.999(3)°, $V = 987.3(1)$ and 970.5(1) Å^3, $Z = 3$, $R_1(I > 2\sigma(I)) = 0.028$ and 0.030, R_w (all data) = 0.079 and 0.094, respectively. The crystal structure is composed of $\{RO_8\}$ and $\{MoO_{n'}\}$ ($n' = 4-6$) polyhedral units. The molybdate units are condensed to give a corrugated $\{Mo_4O_{17}\}_\infty$ chain. The square-antiprismatic $\{RO_8\}$ units share their trigonal and square faces, forming $\{R_2O_{13}\}$ and $\{R_2O_{12}\}$ groups, respectively. A very short $R\cdots R$ distance (3.557(6) Å for R = Nd; 3.4956(6) Å for R = Sm) is achieved in the latter unusual $\{R_2O_{12}\}$ group. A common cationic arrangement was found in all the structures in the $R_2Mo_4O_{15}$ family: a R–R pair with the shortest separation and surrounding 12 Mo atoms. The symmetry of the cationic arrangement was reduced with an increase of atomic number of R, viz. La > Ce, Pr > Nd–Gd ≈ Tb, Ho.

Keywords: Rare-earth molybdate; Rare-earth polyoxomolybdate; Thermal decomposition; Pyrolysis, Crystal structures

1. Introduction

Much interest has been focused on the solid state chemistry and physics of rare earth (R) molybdates because of their potent ferroelectricity/ferroelastisity [1] and remarkable applications to laser hosts [2], phosphors [3–5], ionic conductors [6,7], etc. It is also of interest that R molybdates often exhibit polymorphs due to the flexibility of coordination number and geometry for both R^{3+} and Mo^{6+} centers, realizing 6–12 and 4–7 coordinates [8] respectively, with various coordination polyhedra. For this reason, a replacement of R with other species in R molybdate sometimes gives rise to a drastic structural change. One of such examples is R_2MoO_6 compounds [9], which crystallize in monoclinic (α-form), cubic (β-form), and tetragonal (γ-form) systems depending on the size of R and preparation conditions. A family of $R_2Mo_4O_{15}$ has also been known to exhibit different structures with R = La (monoclinic) [10], R = Ce [11], Pr [12] (triclinic), and R = Tb [13], Ho [14] (monoclinic). However, structures of $R_2Mo_4O_{15}$ in the R = Nd–Gd region were unknown probably due to the difficulty in obtaining single crystals suitable for X-ray structure determination. We have studied polymorphs of the $R_2Mo_4O_{15}$ family using R-containing polyoxomolybdate $[R_2(H_2O)_{12}Mo_8O_{27}]\cdot xH_2O$ as the precursor [13,15], because thermal decomposition of this compound gives well-formed crystals of various R molybdates [16,17]. So far, we have synthesized $R_2Mo_4O_{15}$ with R = Ce, Pr, Eu, Gd, Tb, and Er by 750°C decompositions of the corresponding precursors. The resulting R = Ce and Pr crystals (Unpublished data) are identical to the known Pr [11] and Pr [12] compounds, respectively. The products with R = Tb [13] and Er (Unpublished data) are isomorphous with

*Corresponding author. Fax: +81-(0)45-924-5276.
E-mail address: hnaruke@res.titech.ac.jp (H. Naruke).

0022-4596/03/$ - see front matter © 2003 Elsevier Science (USA). All rights reserved.
doi:10.1016/S0022-4596(03)00131-2

Table 1
Crystallographic data and results for the structural analyses

Formula	β-$La_2Mo_4O_{15}$	$Nd_2Mo_4O_{15}$	$Sm_2Mo_4O_{15}$
Formula weight	901.56	912.23	924.47
Crystal size (mm^3)	$0.04 \times 0.04 \times 0.05$	$0.04 \times 0.05 \times 0.07$	$0.15 \times 0.08 \times 0.07$
Crystal system	Monoclinic	Triclinic	Triclinic
Space group (No.)	$P2_1/a$ (No. 16)	$P\bar{1}$ (No. 2)	$P\bar{1}$ (No. 2)
Unit cell dimensions	$a = 13.8893(5)$ Å	$a = 9.4989(5)$ Å	$a = 9.4076(7)$ Å
	$b = 13.0757(4)$ Å	$b = 11.0088(7)$ Å	$b = 10.9583(8)$ Å
	$c = 20.0927(8)$ Å	$c = 11.5665(6)$ Å	$c = 11.5234(8)$ Å
	—	$\alpha = 104.141(3)^\circ$	$\alpha = 104.225(3)^\circ$
	$\beta = 95.199(2)^\circ$	$\beta = 109.838(3)^\circ$	$\beta = 109.603(3)^\circ$
	—	$\gamma = 108.912(3)^\circ$	$\gamma = 108.999(3)^\circ$
Volume	3634.1(2)	987.3(1) $Å^3$	970.5(1) $Å^3$
Z	12	3	3
D_{calc}	4.943 g cm^{-3}	4.602 g cm^{-3}	4.745 g cm^{-3}
$\mu(MoK_\alpha)$	109.55 cm^{-1}	115.01 cm^{-1}	127.77 cm^{-1}
$F(000)$	4824	1224	1236
Crystal color and habit	Colorless, block	Pale purple, block	Pale yellow, block
No. of reflections			
Total	11003	11645	8019
Unique (R_{int})	10571 (0.072)	5660 (0.032)	5601 (0.030)
Used for refinement	10562	5659	5600
Transmission factor	0.5660–0.6185	0.4488–0.6312	0.1531–0.3929
Secondary extinction coeff.	—	0.0015(2)	0.0099(4)
No. of variables	568	287	287
R_w (all data)	0.116[a,b]	0.079[a,c]	0.094[a,c]
R_1[d]	0.048	0.028	0.030
Maximum shift/error	0.001	0.001	0.001
Goodness-of-fit	0.98	1.14	1.49
$\Delta\rho_{max}$	4.38 $e^-Å^{-3}$	2.00 $e^-Å^{-3}$	3.37 $e^-Å^{-3}$
	(0.25 Å from La5)	(1.62 Å from Nd3)	(0.81 Å from Sm2)
$\Delta\rho_{min}$	–4.29 $e^-Å^{-3}$	—1.83 $e^-Å^{-3}$	—2.84 $e^-Å^{-3}$
	(2.28 Å from La6)	(2.13 Å from Nd1)	(0.05 Å from Sm2)

[a] $R_w = \{\sum[w(F_o^2 - F_c^2)^2]/\sum[w(F_o^2)^2]\}^{1/2}$.
[b] $w = [\{0.001F_o^2 + 0.5\sigma_c^2(F_o) + 0.001\}/(4F_o^2)]^{-1}$.
[c] $w = [\sigma_c^2(F_o^2) + \{p(\mathrm{Max}(F_o^2,0) + 2F_c^2)/3\}^2]^{-1}$ with $p = 0.01$.
[d] $R_1 = \sum||F_o| - |F_c||/\sum|F_o|$ for $I > 2\sigma(I)$.

$Ho_2Mo_4O_{15}$ [14]. Recently, we characterized the structure of R = Eu and Gd phases for the first time [15]. This structure is more complicated than other $R_2Mo_4O_{15}$ phases, comprising asymmetric unit of $R_3Mo_6O_{22.5}$, and therefore, can also be formulated as $R_6Mo_{12}O_{45}$ [15].

In this study, synthesis of $R_2Mo_4O_{15}$ with R = Nd and Sm is carried out by using Nd and Sm precursors. These compounds have been known to exist [18,19], but their structures undetermined. X-ray structural analysis revealed that the R = Nd and Sm compounds are isomorphous with the R = Eu and Gd analogs [15]. This enables us to discuss the size-effect of R on the $R_2Mo_4O_{15}$ (R = Nd, Sm, Eu, Gd) structures. In addition, we report here the crystal structure of the R = La compound. This novel phase (denoted as the β-form hereafter) is an isomer of the previously known $La_2Mo_4O_{15}$ (denoted as the α-form) [10]. Structures of the two $La_2Mo_4O_{15}$ forms are compared in detail. Finally, we attempt to compare all the structures in the $R_2Mo_4O_{15}$ family in view of their cationic arrangements and extract a common structural feature.

2. Experimental section

2.1. Synthesis

The precursor R polyoxomolybdate, $[R_2(H_2O)_{12}Mo_8O_{27}] \cdot xH_2O$ (R = La, Nd, Sm), was prepared by acidification (pH 3.0) of a stoichiometric mixture of R^{3+} and $[MoO_4]^{2-}$ in a diluted aqueous solution [13,15,20]. A powder sample of $[R_2(H_2O)_{12}Mo_8O_{27}] \cdot xH_2O$ (100 mg) was placed in a boat-shaped alumina container, and fired in air at 750°C in a furnace for 4 h (for Nd and Sm) and 8 h (for La), and then quenched by exposure to ambient temperature (ca. 20–25°C). The set up of the furnace and firing conditions were described previously [16] in detail. In all cases, $R_2Mo_4O_{15}$ crystallized on the surface of a colored (greenish gray) glassy substance formed by the decomposition and melting of the precursor.

As a result of the $[La_2(H_2O)_{12}Mo_8O_{27}] \cdot xH_2O$ decomposition, colorless transparent prismatic crystals were initially formed soon after the sample was removed from

Table 2
Positional and displacement parameters of β-$La_2Mo_4O_{15}$

Atom	x	y	z	U_{eq} (Å^2)
La1	0.94503(5)	1.13262(5)	0.29061(3)	0.0113(2)
La2	0.78408(5)	1.11754(5)	0.45406(3)	0.0111(2)
La3	0.85417(5)	0.61485(6)	0.37594(4)	0.0130(2)
La4	0.67971(5)	0.84329(6)	0.05391(3)	0.0120(2)
La5	0.52330(5)	0.87341(5)	0.20611(3)	0.0096(1)
La6	0.61129(5)	0.37290(5)	0.13392(3)	0.0091(1)
Mo1	1.06607(7)	1.15360(8)	0.48419(5)	0.0099(2)
Mo2	0.91157(7)	0.91520(8)	0.18002(5)	0.0104(2)
Mo3	0.76959(7)	0.90618(8)	0.33866(5)	0.0102(2)
Mo4	0.62669(7)	0.90243(8)	0.48878(5)	0.0101(2)
Mo5	0.71807(7)	1.08236(8)	0.14015(5)	0.0102(2)
Mo6	0.51534(7)	1.08794(8)	0.35296(5)	0.0099(2)
Mo7	0.72393(7)	0.64854(8)	0.20950(5)	0.0099(2)
Mo8	0.57735(7)	0.64348(8)	0.36628(5)	0.0101(2)
Mo9	0.90092(7)	0.66196(8)	0.02060(5)	0.0110(2)
Mo10	0.62612(8)	0.56357(8)	−0.01619(5)	0.0118(2)
Mo11	0.71643(7)	0.34067(8)	0.32771(5)	0.0107(2)
Mo12	0.40452(7)	0.15709(8)	0.14358(5)	0.0103(2)
O1	0.9768(7)	1.3104(7)	0.3013(5)	0.0209(2)
O2	1.0386(6)	0.9752(7)	0.3363(4)	0.0162(2)
O3	0.9637(6)	1.1571(7)	0.4231(4)	0.0087(2)
O4	0.7911(6)	1.2320(6)	0.3312(5)	0.0134(2)
O5	0.8351(6)	1.0223(7)	0.3545(5)	0.0152(2)
O6	0.8012(7)	1.0908(7)	0.2097(4)	0.0188(2)
O7	0.8076(6)	1.1483(6)	0.5821(4)	0.0124(2)
O8	0.8237(7)	1.2962(7)	0.4719(5)	0.0165(2)
O9	0.6366(6)	1.2376(7)	0.5041(4)	0.0158(2)
O10	0.8764(7)	0.9647(6)	0.5029(4)	0.0147(2)
O11	0.6665(6)	1.0285(6)	0.5185(4)	0.0110(2)
O12	0.6389(7)	1.1000(7)	0.3727(5)	0.0187(2)
O13	1.0198(6)	0.6225(7)	0.4418(4)	0.0168(2)
O14	0.8281(7)	0.7894(7)	0.3544(5)	0.0210(2)
O15	0.6820(7)	0.6393(7)	0.2904(4)	0.0201(2)
O16	0.7883(7)	0.4512(7)	0.3329(5)	0.0197(2)
O17	0.6333(7)	1.0521(7)	0.0283(5)	0.0220(2)
O18	0.5997(8)	0.8508(7)	−0.0564(5)	0.0238(2)
O19	0.8052(7)	0.7021(7)	0.0655(5)	0.0208(2)
O20	0.6063(6)	0.6603(7)	0.0384(4)	0.0164(2)
O21	0.8228(6)	0.9389(7)	0.1097(4)	0.0169(2)
O22	0.6507(6)	0.9688(6)	0.1493(4)	0.0086(2)
O23	0.5068(6)	0.8609(6)	0.0781(4)	0.0096(2)
O24	0.6766(6)	0.7602(6)	0.1694(4)	0.0144(2)
O25	0.4598(7)	1.0445(7)	0.1757(4)	0.0154(2)
O26	0.4768(7)	0.6953(7)	0.1675(5)	0.0194(2)
O27	0.3512(6)	0.8499(7)	0.2280(5)	0.0178(2)
O28	0.6692(7)	0.9048(8)	0.2812(4)	0.0198(2)
O29	0.4860(6)	0.9695(6)	0.3118(4)	0.0139(2)
O30	0.5325(6)	0.7462(7)	0.3185(5)	0.0193(2)
O31	0.4929(6)	0.4820(7)	0.1976(4)	0.0151(2)
O32	0.7846(7)	0.3396(8)	0.1646(5)	0.0249(3)
O33	0.4857(6)	0.4663(7)	0.0619(4)	0.0183(2)
O34	0.5817(7)	0.2631(8)	0.0325(5)	0.0219(3)
O35	0.6400(6)	0.1812(7)	0.1512(4)	0.0161(2)
O36	0.6297(6)	0.3457(7)	0.2571(4)	0.0169(2)
O37	0.6884(7)	0.5416(7)	0.1632(5)	0.0204(2)
O38	0.6819(6)	0.4600(7)	0.0272(4)	0.0123(2)
O39	0.4629(6)	0.2723(7)	0.1730(4)	0.0141(2)
O40	1.1417(7)	1.1620(7)	0.3927(4)	0.0159(2)
O41	0.9961(7)	1.1521(8)	0.5593(5)	0.0217(2)
O42	0.5434(7)	0.9137(7)	0.5723(4)	0.0192(2)
O43	0.8523(6)	0.8966(6)	0.2519(4)	0.0140(2)
O44	0.7082(7)	0.9120(7)	0.4189(4)	0.0176(2)
O45	0.7032(6)	0.6332(6)	−0.0728(4)	0.0113(2)

Table 3
Selected interatomic distances (Å) in β-$La_2Mo_4O_{15}$

La1–O1	2.372(9)	La5–O22	2.520(8)	Mo5–O6	1.735(9)
La1–O2	2.560(9)	La5–O23	2.566(8)	Mo5–O17	2.473(9)
La1–O3	2.670(9)	La5–O24	2.749(9)	Mo5–O21	2.484(9)
La1–O4	2.691(9)	La5–O25	2.461(8)	Mo5–O22	1.774(8)
La1–O5	2.533(8)	La5–O26	2.520(9)	Mo5–O35^{vii}	1.715(8)
La1–O6	2.518(9)	La5–O27	2.488(9)	Mo5–O45^{iii}	1.933(8)
La1–O31^{i}	2.530(8)	La5–O28	2.449(9)	Mo6–O1^{viii}	1.740(9)
La1–O36^{i}	2.725(9)	La5–O29	2.560(9)	Mo6–O12	1.733(9)
La1–O39^{i}	2.702(9)	La5–O30	2.798(9)	Mo6–O29	1.785(9)
La2–O3	2.676(8)	La6–O31	2.600(9)	Mo6–O42^{ix}	1.774(9)
La2–O4	2.896(9)	La6–O32	2.469(9)	Mo7–O15	1.779(9)
La2–O5	2.513(9)	La6–O33	2.485(9)	Mo7–O24	1.766(8)
La2–O7	2.596(8)	La6–O34	2.496(9)	Mo7–O27^{i}	1.774(9)
La2–O8	2.419(9)	La6–O35	2.557(8)	Mo7–O37	1.726(9)
La2–O9	2.836(9)	La6–O36	2.490(9)	Mo8–O2^{vi}	1.733(9)
La2–O10	2.524(8)	La6–O37	2.499(9)	Mo8–O7^{ii}	1.826(8)
La2–O11	2.466(8)	La6–O38	2.690(8)	Mo8–O15	2.201(9)
La2–O12	2.489(9)	La6–O39	2.625(9)	Mo8–O30	1.734(9)
La2–O44	2.949(9)	Mo1–O3	1.793(8)	Mo8–O41^{ii}	1.888(9)
La3–O7^{ii}	2.508(8)	Mo1–O9^{iv}	1.753(9)	Mo9–O17	1.781(9)
La3–O9^{ii}	2.889(9)	Mo1–O1^{v}	1.749(8)	Mo9–O19	1.754(9)
La3–O11^{ii}	2.442(8)	Mo1–O40	2.201(8)	Mo9–O23^{i}	1.811(8)
La3–O13	2.550(8)	Mo1–O41	1.868(9)	Mo9–O34^{iii}	1.73(1)
La3–O14	2.345(9)	Mo2–O21	1.817(8)	Mo10–O20	1.714(9)
La3–O15	2.83(1)	Mo1–O26^{i}	1.736(9)	Mo10–O33^{xi}	1.774(9)
La3–O16	2.454(9)	Mo1–O31^{i}	1.771(9)	Mo10–O38	1.752(8)
La3–O27	3.005(9)	Mo1–O43	1.743(8)	Mo10–O45	1.868(8)
La3–O29^{i}	2.581(9)	Mo3–O5	1.783(9)	Mo11–O4^{xii}	1.757(8)
La4–O17	2.84(1)	Mo3–O14	1.75(1)	Mo11–O16	1.754(9)
La4–O18	2.390(9)	Mo3–O28	1.728(9)	Mo11–O36	1.778(9)
La4–O19	2.535(9)	Mo3–O43	2.177(8)	Mo11–O40^{vi}	1.740(9)
La4–O20	2.608(9)	Mo3–O44	1.892(9)	Mo12–O18^{xi}	1.750(9)
La4–O21	2.523(9)	Mo4–O8^{ii}	1.712(9)	Mo12–O25^{xii}	1.756(9)
La4–O22	2.582(8)	Mo4–O11	1.823(8)	Mo12–O32^{xiii}	1.76(1)
La4–O23	2.504(8)	Mo4–O13^{vi}	1.717(8)	Mo12–O39	1.785(9)
La4–O24	2.565(8)	Mo4–O42	2.127(9)		
La4–O38^{iii}	3.041(9)	Mo4–O44	1.887(9)		

Note. (i) $x+1/2,\ -y+3/2,\ z$; (ii) $-x+3/2,\ y-1/2,\ -z+1$; (iii) $-x+3/2,\ y;1/2,\ -z$; (iv) $x+1/2,\ -y;5/2,\ z$; (v) $2-x,\ 2-y,\ 1-z$; (vi) $x-1/2,\ -y+3/2,\ z$; (vii) $x,\ y;1,\ z$; (viii) $x-1/2,\ -y+5/2,\ z$; (ix) $1-x,\ 2-y,\ 1-z$; (x) $-x+3/2,\ y-1/2,\ -z$; (xi) $1-x,\ 1-y,\ -z$; (xii) $x,\ y-1,\ z$; (xiii) $x-1/2,\ -y+1/2,\ z$.

the furnace. However, on cooling to room temperature, most of the crystals were exfoliated from the glassy phase, and changed to opaque polycrystalline, whereas a few transparent crystals remained. The former polycrystalline phase was identified as α-$La_2Mo_4O_{15}$ from powder X-ray diffraction analysis, and the latter crystals were the novel β-$La_2Mo_4O_{15}$ phase.

$R_2Mo_4O_{15}$ (R = Nd, Sm) crystallized as clear pale purple and pale yellow blocks in the glassy phases, respectively. It should be noted that when the precursor was fired in a virgin alumina container, no crystal was formed in the glassy phase in most cases. Repeated use of the same container (product was mechanically removed before each reaction) was effective in enhancing the crystallization. Because no contamination of Al from the container could be detected in the products

Table 4
Positional and displacement parameters of $R_2Mo_4O_{15}$ (R = Nd and Sm)

Atom	x	y	z	U_{eq} (Å^2)	x	y	z	U_{eq} (Å^2)
	$Nd_2Mo_4O_{15}$				$Sm_2Mo_4O_{15}$			
*R*1	0.21847(3)	0.05692(3)	0.59130(3)	0.01017(7)	0.21648(4)	0.05654(3)	0.59053(3)	0.01010(7)
R2	−0.23323(3)	−0.22103(3)	0.82577(3)	0.00911(7)	−0.23473(4)	−0.22234(3)	0.82501(3)	0.00918(7)
R3	0.33421(3)	−0.65847(3)	0.20097(3)	0.00870(6)	−0.33574(4)	−0.65935(3)	0.20119(3)	0.00888(7)
Mo1	0.58503(6)	0.22471(5)	0.48145(5)	0.0099(1)	0.58459(6)	0.22374(5)	0.48115(5)	0.0100(1)
Mo2	0.06742(6)	−0.13358(5)	0.20369(5)	0.01045(10)	0.06708(6)	−0.13266(5)	0.20314(5)	0.0103(1)
Mo3	−0.08502(6)	−0.31050(5)	0.55263(4)	0.00946(10)	−0.08546(6)	−0.31135(5)	0.55248(5)	0.0094(1)
Mo4	0.90972(6)	0.46615(5)	0.81857(4)	0.00849(10)	0.91054(6)	0.46702(5)	0.81832(5)	0.0087(1)
Mo5	−0.26744(6)	−0.98112(5)	0.07796(5)	0.00918(10)	−0.26708(6)	−0.98144(5)	0.07939(5)	0.0093(1)
Mo6	−0.46872(6)	−0.56615(5)	−0.13184(5)	0.00968(10)	−0.47204(6)	−0.56595(5)	−0.13258(5)	0.0093(1)
O1	0.4189(5)	0.1656(5)	0.5196(4)	0.019(1)	0.4177(6)	0.1646(5)	0.5204(5)	0.018(1)
O2	0.3395(5)	0.2884(4)	0.7592(4)	0.0166(10)	0.3352(6)	0.2870(4)	0.7564(4)	0.017(1)
O3	0.2895(6)	0.0125(5)	0.7859(4)	0.018(1)	0.2888(6)	0.0137(5)	0.7850(4)	0.018(1)
O4	−0.0337(5)	−0.1579(4)	0.5141(4)	0.0142(9)	−0.0347(6)	−0.1599(4)	0.5130(4)	0.0148(10)
O5	0.0321(6)	−0.0679(5)	0.3416(4)	0.018(1)	0.0309(6)	−0.0671(4)	0.3417(4)	0.016(1)
O6	0.6568(6)	0.0990(5)	0.4497(5)	0.021(1)	0.6580(7)	0.0984(5)	0.4513(5)	0.023(1)
O7	0.5250(5)	0.2686(4)	0.3407(4)	0.0147(9)	0.5260(5)	0.2669(5)	0.3389(4)	0.0145(10)
O8	0.7525(6)	0.3819(5)	0.6196(4)	0.0189(10)	0.7527(6)	0.3824(5)	0.6190(4)	0.018(1)
O9	1.0000	0.5000	1.0000	0.023(2)	1.0000	0.5000	1.0000	0.021(2)
O10	0.2168(5)	0.0063(4)	0.2000(5)	0.018(1)	0.2195(6)	0.0089(5)	0.1990(5)	0.018(1)
O11	0.1499(6)	−0.2550(4)	0.2254(5)	0.018(1)	0.1509(6)	−0.2541(4)	0.2258(5)	0.016(1)
O12	−0.1164(6)	−0.2142(4)	0.0534(4)	0.0184(10)	−0.1189(6)	−0.2155(5)	0.0515(5)	0.018(1)
O13	0.1005(6)	−0.3025(5)	0.6648(5)	0.020(1)	0.1024(6)	−0.3021(5)	0.6643(5)	0.019(1)
O14	−0.2225(6)	−0.3078(5)	0.6223(4)	0.019(1)	−0.2239(6)	−0.3072(5)	0.6224(5)	0.019(1)
O15	−0.1083(6)	−0.3815(4)	0.8327(4)	0.017(1)	−0.1074(6)	−0.3793(5)	0.8328(5)	0.017(1)
O16	−0.1872(6)	−0.4617(5)	0.4065(5)	0.021(1)	−0.1895(6)	−0.4635(5)	0.4059(5)	0.018(1)
O17	−0.0869(5)	−0.4999(5)	0.2012(4)	0.017(1)	−0.0894(6)	−0.5007(5)	0.2000(5)	0.018(1)
O18	−0.4029(6)	−0.5516(5)	0.0410(4)	0.017(1)	−0.4068(6)	−0.5541(5)	0.0408(4)	0.017(1)
O19	−0.3333(5)	−0.8537(5)	0.0508(4)	0.0167(10)	−0.3325(6)	−0.8531(5)	0.0530(5)	0.016(1)
O20	−0.0577(5)	−0.9233(5)	0.1079(5)	0.020(1)	−0.0555(6)	−0.9214(5)	0.1116(5)	0.019(1)
O21	−0.3858(5)	−1.1430(4)	−0.0663(4)	0.0140(9)	−0.3840(5)	−1.1447(4)	−0.0658(4)	0.0126(9)
O22	−0.3264(6)	−0.6129(5)	−0.1688(5)	0.021(1)	−0.3264(6)	−0.6129(5)	−0.1680(5)	0.021(1)
O23	−0.4477(5)	−0.4238(4)	−0.1877(4)	0.0134(9)	−0.4498(5)	−0.4246(4)	−0.1921(4)	0.0124(9)

(analyzed by energy dispersive X-ray measurement), we assume that gradual nucleation of $R_2Mo_4O_{15}$ occurs on the container surface through the repeated exposure to the melt. An attempt to use a silica container resulted in the same crystallization-enhancing effect. Similar behavior has been pointed out in crystallization of $R_4Mo_7O_{27}$ (R = Eu(16), Gd(17)), $Eu_6Mo_{10}O_{39}$ [16], and $Tb_2Mo_4O_{15}$ [13].

2.2. Single crystal X-ray crystallography

Single crystals of $R_2Mo_4O_{15}$ (R = La, Nd, Sm) were fixed on glass fibers and mounted on a Rigaku RAXIS-RAPID imaging-plate X-ray diffractometer with graphite-monochromatized Mo$K\alpha$ radiation (0.71069 Å). Structures were solved by SIR92 [21] and refined with full-matrix least-squares techniques. All atoms were refined anisotropically. Secondary extinction coefficients [22] were refined for R = Nd and Sm. Numerical absorption correction was done using SHAPE [23] and NUMABS [24]. All calculations were carried out using structure analysis software packages, Crystal structure [25] for R = La, and teXsan [26] for R = Nd and Sm. The complete crystallographic data and results of the refinements are summarized in Table 1. Atomic coordinates and selected interatomic distances are listed in Tables 2–5. Further details of the crystal structures can be obtained from the Fachinformationszetrum Karlsruhe, 76344 Eggenstein-Leopoldshafen, Germany, (fax: (49)7247-808-666; email: crysdata@fiz-karlsruhe.de: URL: http://www.fiz-karlsruhe.de) on quoting the depository numbers CSD-413030 (β-$La_2Mo_4O_{15}$), CSD-413028 ($Nd_2Mo_4O_{15}$) and CSD-413029 ($Sm_2Mo_4O_{15}$).

Powder X-ray diffraction (XRD) patterns were obtained using the same diffractometer because the

Table 5
Selected interatomic distances (Å) in $R_2Mo_4O_{15}$ (R = Nd and Sm)

	R = Nd	R = Sm
*R*1–O3	2.342(4)	2.326(4)
*R*1–O2	2.399(4)	2.374(4)
*R*1–O1	2.413(4)	2.382(4)
*R*1–O6^{i}	2.424(4)	2.407(5)
*R*1–O4	2.444(4)	2.429(4)
*R*1–O4^{ii}	2.506(4)	2.487(4)
*R*1–O5	2.525(4)	2.510(4)
*R*1–O5^{ii}	2.771(4)	2.718(5)
*R*2–O14	2.364(4)	2.341(5)
*R*2–O23^{iii}	2.414(4)	2.376(4)
*R*2–O10^{ii}	2.416(4)	2.386(4)
*R*2–O20^{iv}	2.423(4)	2.401(5)
*R*2–O15	2.430(4)	2.398(4)
*R*2–O21^{v}	2.431(4)	2.391(4)
*R*2–O12^{iii}	2.456(4)	2.439(4)
*R*2–O7^{ii}	2.571(4)	2.553(4)
*R*3–O16	2.358(4)	2.340(5)
*R*3–O19	2.416(4)	2.392(5)
*R*3–O17	2.429(4)	2.409(4)
*R*3–O18	2.444(4)	2.432(4)
*R*3–O21^{vi}	2.456(4)	2.430(4)
*R*3–O13^{iv}	2.476(4)	2.458(4)
*R*3–O23^{vii}	2.491(4)	2.458(4)
*R*3–O7^{viii}	2.540(4)	2.488(4)
Mo1–O6	1.746(4)	1.740(5)
Mo1–O1	1.748(4)	1.746(5)
Mo1–O7	1.772(4)	1.778(4)
Mo1–O8	1.793(4)	1.792(4)
Mo2–O12	1.744(4)	1.753(5)
Mo2–O10	1.745(4)	1.760(4)
Mo2–O5	1.771(4)	1.772(5)
Mo2–O11	1.781(4)	1.783(4)
Mo3–O16	1.742(4)	1.742(5)
Mo3–O14	1.756(4)	1.753(5)
Mo3–O13	1.757(4)	1.757(4)
Mo3–O4	1.800(4)	1.786(4)
Mo4–O17^{i}	1.709(4)	1.698(5)
Mo4–O15^{ix}	1.714(4)	1.719(4)
Mo4–O9	1.8621(4)	1.8628(5)
Mo4–O8	2.028(4)	2.027(4)
Mo4–O11^{i}	2.087(4)	2.092(4)
Mo4–O22^{x}	2.198(4)	2.190(5)
Mo5–O3^{iv}	1.756(4)	1.745(4)
Mo5–O20	1.759(4)	1.751(5)
Mo5–O19	1.763(4)	1.760(4)
Mo5–O21	1.788(4)	1.795(4)
Mo6–O22	1.735(5)	1.743(5)
Mo6–O2^{xi}	1.742(4)	1.746(4)
Mo6–O23	1.814(4)	1.822(4)
Mo6–O18	1.829(4)	1.839(4)
Mo6–O18^{vii}	2.345(4)	2.291(5)
*R*1⋯*R*1^{ii}	3.5557(6)	3.4956(6)
*R*2⋯*R*3^{xii}	3.7605(4)	3.6984(5)

Note. (i) $1-x, -y, 1-z$; (ii) $-x, -y, 1-z$; (iii) $x, y, 1+z$; (iv) $-x, -1-y, 1-z$; (v) $x, 1+y, 1+z$; (vi) $-1-x, -2-y, -z$; (vii) $-1-x, -1-y, -z$; (viii) $-1+x, -1+y, z$; (ix) $1+x, 1+y, z$; (x) $1+x, 1+y, 1+z$; (xi) $-1+x, -1+y, -1+z$; (xii) $-1-x, -1-y, 1-z$.

sample amounts are too small to perform usual powder X-ray diffractometry. A powder sample, sealed in a glass capillary, was exposed to a 0.3 mm-collimated X-ray beam for 15–20 min. Intensity of the resulting ring image was integrated and converted to a 2θ-intensity plot.

3. Results and discussion

3.1. Structural description of β-$La_2Mo_4O_{15}$ and comparison with the α-form

Fig. 1 represents the structure of β-$La_2Mo_4O_{15}$. The asymmetric unit contains 6 La, 12 Mo, and 45 O atoms (Table 2). Each La atom except for La(2) is surrounded by 9 O atoms with the La–O distances ranging from 2.345(9) to 3.041(9) Å (Fig. 1b). La(2) achieves 10-coordinate with the longest La(2)–O(44) distance of 2.949(9) Å. All the $\{LaO_n\}$ polyhedra are connected together into a linear chain running along the $[10\bar{1}]$ direction (Fig. 1b). In the chain, the six $\{LaO_n\}$ polyhedra share two or three bridging O atoms to form a $\{La_6O_{39}\}$ unit, and the units are linked by a bridging O(38) atom. Inter-La distances in the chain are indicated in Fig. 1b, in which the short (3.928(1)–4.070(1) Å) and long (4.317–4.980(1) Å) distances are repeated alternately, giving a ⋯La(4)–La(5)⋯La(3)–La(2)⋯La(1)–La(6)⋯ framework in which the short/long distances are denoted with solid/dotted lines. The Mo and surrounding O atoms form $\{Mo(2,6,7,9,10–12)O_4\}$ tetrahedra, $\{Mo(1,3,4,8)O_5\}$ trigonal bipyramids, and $\{Mo(5)O_6\}$ octahedron (Fig. 1c). The $\{MoO_4\}$ tetrahedra are nearly regular possessing Mo–O distances of 1.726(9)–1.826(8)Å and O–Mo–O angles of 99.5(4)–115.3(4)°. Each of the $\{MoO_5\}$ trigonal bipyramids comprises four short Mo–O bonds (1.712(9)–1.887(9) Å) and a longer (2.127(9)–2.201(8) Å) axial Mo–O bond. In the $\{MoO_5\}$ polyhedra, the O–Mo–O angles for the axial and equatorial sets are 171.3(4)–176.4(4) and 113.1(4)–125.0(4)°, respectively. Much distortion is observed in the $\{Mo(5)O_6\}$ octahedron as demonstrated by the large distributions of the *cis*-(70.9(3)–106.8(4)°) and *trans*-(134.3(4)–173.0(4)°) O–Mo–O angles (ideally 90° and 180°, respectively) and the Mo–O lengths (1.715(8)–2.484(9) Å). The $\{Mo(7,11)O_4\}$ and $\{Mo(1,8)O_5\}$ polyhedra are condensed to a linear $\{Mo_4O_{15}\}$ chain by sharing axial O(15,40,41) atoms. Similarly, the $\{Mo(2,6)O_4\}$ and $\{Mo(3,4)O_5\}$ polyhedra form a tetrameric $\{Mo_4O_{15}\}$ chain, which is also attached to a $\{Mo(5,9,10)O_{12}\}$ group to form a larger $\{Mo_7O_{26}\}$ group. Both linear $\{Mo_4O_{15}\}$ chains, as well as the $\{La_6O_{39}\}_\infty$ chain, lie along the $[10\bar{1}]$ direction.

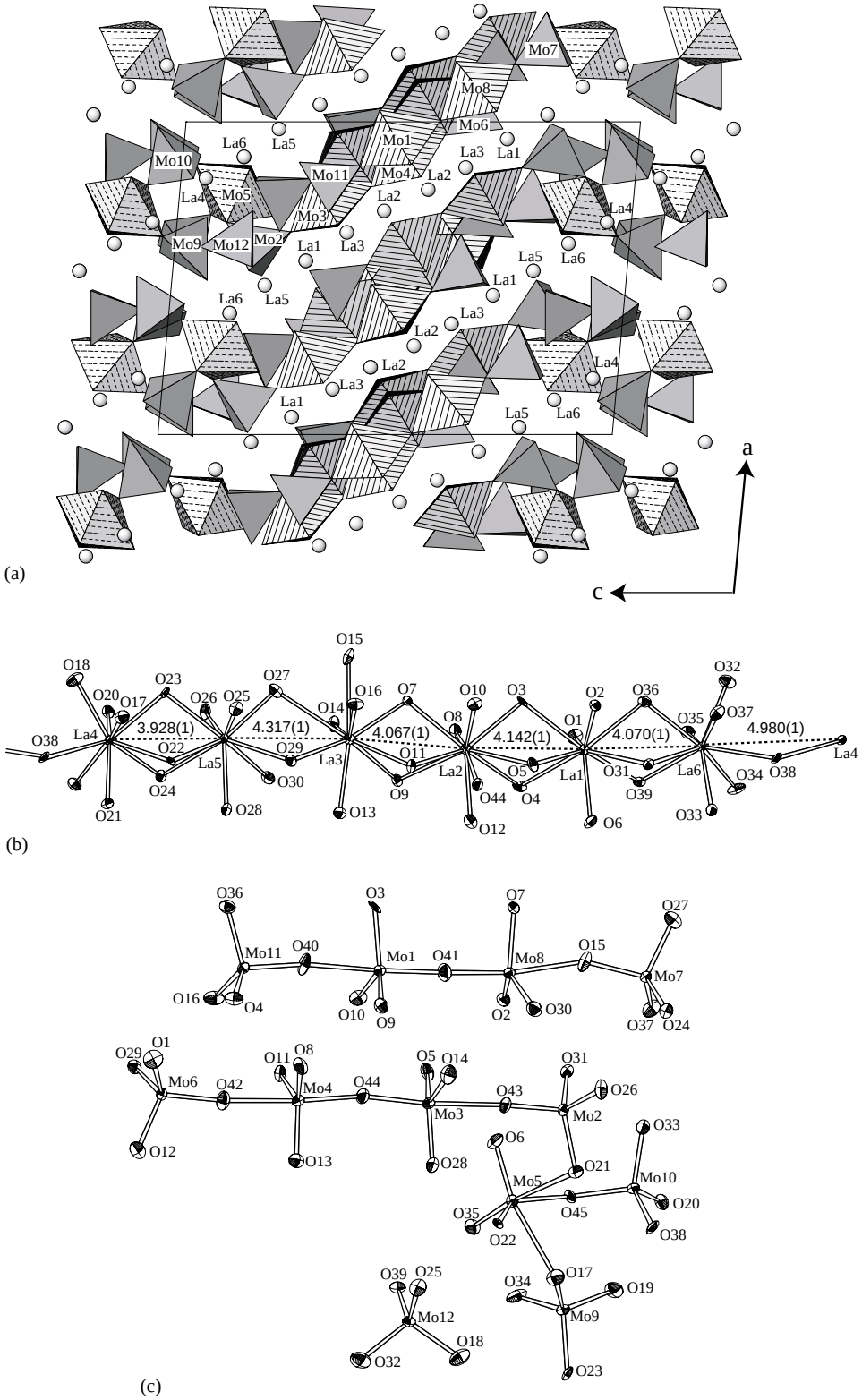

Fig. 1. (a) Crystal structure of β-$La_2Mo_4O_{15}$ with $\{MoO_n\}$-polyhedral representation. The spheres denote La. The $\{MoO_6\}$ and $\{MoO_5\}$ groups are shown with cross- and line-hatched polyhedra. (b) $\{La_6O_{39}\}_\infty$ chain. (c) $\{MoO_4\}$, $\{Mo_4O_{15}\}$, and $\{Mo_7O_{26}\}$ groups. The thermal ellipsoids are drawn at the 50% probability level. For clarity, all symmetry operations are omitted.

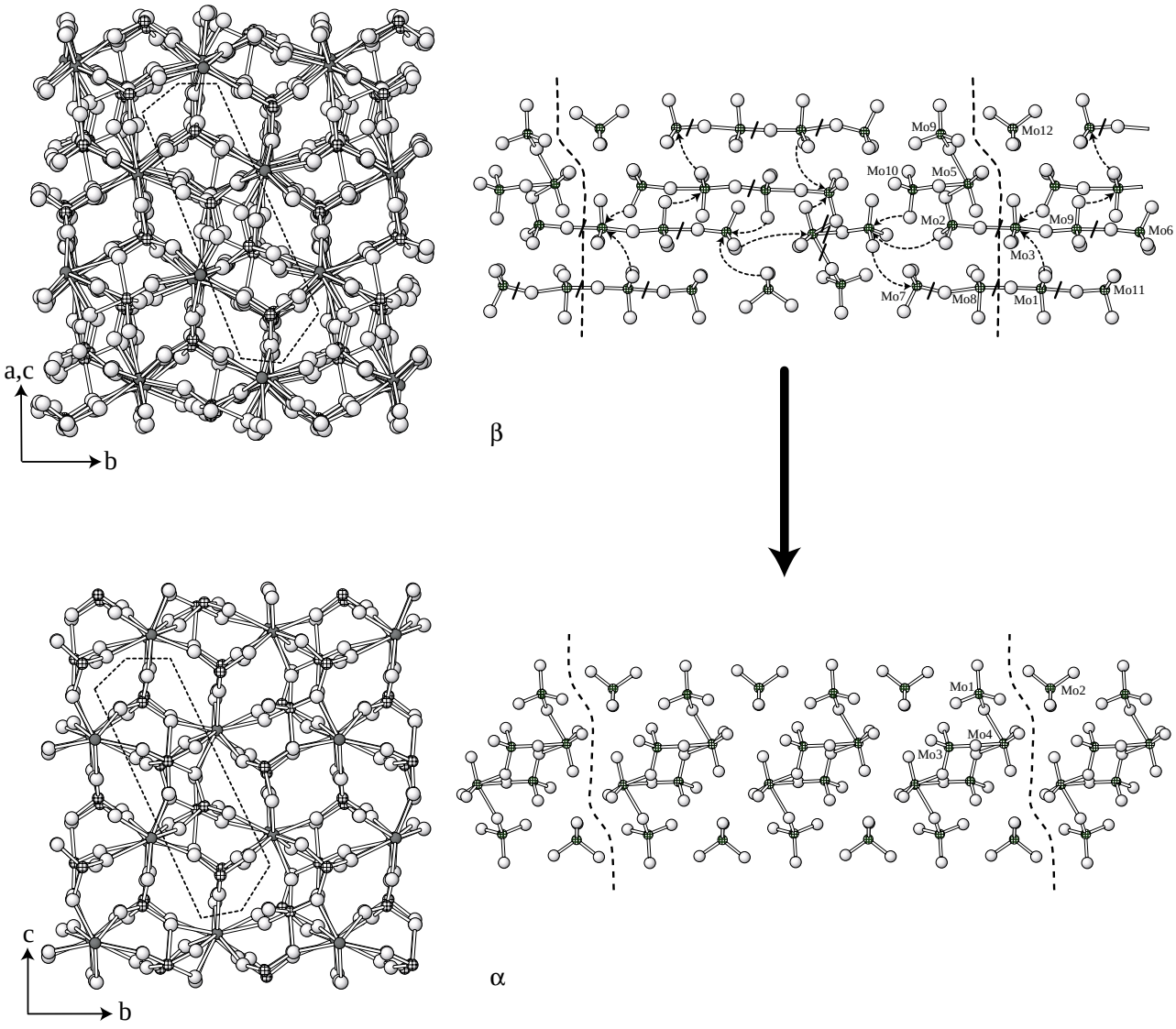

Fig. 2. Ball-and-stick models of β-(top-left) and α-$La_2Mo_4O_{15}$ (bottom-left) structures viewed along [100] and [10$\bar{1}$] directions. La, Mo, and O atoms are represented with dark, cross-hatched, and light-gray spheres, respectively. Side views of the molybdate groups (enclosed by the dashed line in left) are shown in right. The dashed arrows and bold slashes on top-right denote Mo–O bond formation and destruction in $\beta \rightarrow \alpha$ transformation (see text).

Only the $\{Mo(2)O_4\}$ tetrahedron is isolated from other molybdates.

The α- and β-$La_2Mo_4O_{15}$ structures are compared in Fig. 2. As shown in Fig. 2(left), the arrangement of the $\{LaO_n\}$ and $\{MoO_n\}$ polyhedra in the two forms bears a marked resemblance when one views the structures along the [100] and [10$\bar{1}$] directions, respectively. The unit cell of the β-form can be related to that of the α-form by the transformation $a_\alpha \approx (a_\beta - c_\beta)/3$, $b_\alpha \approx b_\beta$, $c_\alpha \approx (a_\beta + c_\beta)/2$. Like the β-form, the α-form also includes a linear lanthanate chain $\{La_2O_{14}\}_\infty$, which is formed by polymerization of two different $\{La(1,2)O_9\}$ polyhedra alternately through one and three bridging O atoms with a long (5.118 Å) and short (3.928 Å) La$\cdots$La separations [10], respectively (figure not shown). Although the resulting La framework ($\cdots$La1–La2$\cdots$La1–La2$\cdots$) is similar to that in the β-form, the chain is 6.5% expanded as compared with the β-form (calculated from $(3 \times 9.032)/25.435$ where 9.032 and 25.435 Å denote the unit lengths in the $\{La_2O_{14}\}_\infty$ (α) and $\{La_6O_{39}\}_\infty$ (β) chains, respectively). In order to compare the molybdate groups, we paid attention on the four $\{MoO_n\}$-columns enclosed by dashed lines in Fig. 2(left); and the side views of the columns are represented in Fig. 2(right). In the lattice, the molybdate groups are arranged in belt-shape in both forms. The α-form has $\{Mo_6O_{22}\}$ and $\{MoO_4\}$ groups, and the former is constructed of four $\{MoO_4\}$ tetrahedra and two $\{MoO_6\}$ octahedra [10]. It should be noted that the arrangement of the Mo centers is similar in the two

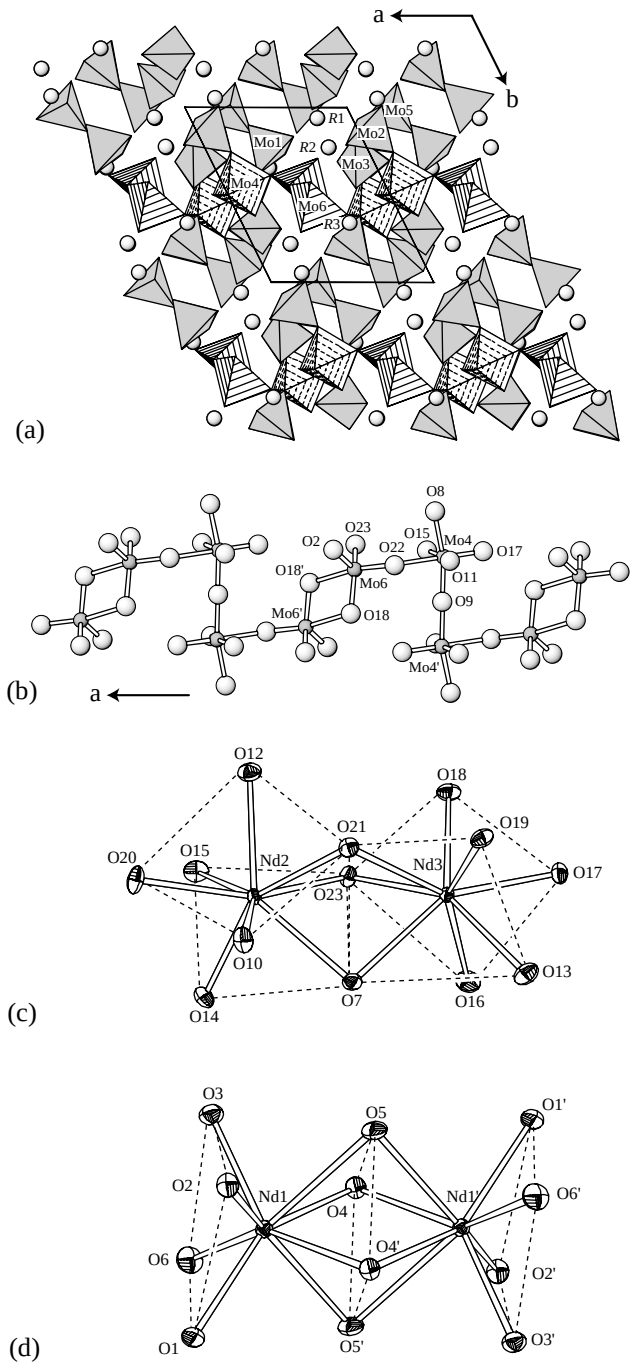

Fig. 3. (a) Crystal structure of $R_2Mo_4O_{15}$ with $\{MoO_n\}$-polyhedral representation. The spheres denote the R atoms. The $\{Mo(4)O_6\}$ and $\{Mo(6)O_5\}$ groups are shown with dash- and line-hatched polyhedra. (b) Ball-and-Stick model of the $\{Mo_4O_{17}\}_\infty$ chain. (c) $\{Nd_2O_{13}\}$ and (d) $\{Nd_2O_{12}\}$ groups. The thermal ellipsoids are drawn at the 50% probability level. Squares in the $\{NdO_8\}$ square-antiprisms in (c) and (d) are drawn with broken lines. For clarity, all symmetry operations on the labels are denoted with a prime (′) without using symmetry code numbers.

forms. Furthermore, the molybdate structure in the α-form is partially maintained in the β-form: linkage and connection of $\{Mo(1)O_4\}$, $\{Mo(4)O_6\}$, $\{Mo(3)O_4\}$, and $\{Mo(2)O_4\}$ in the α-form agree well with those of $\{Mo(9)O_4\}$, $\{Mo(5)O_6\}$, $\{Mo(10)O_4\}$, and $\{Mo(12)O_4\}$ in the β-form, respectively. Fig. 2(top-right) also represents the possible mechanism of the $\beta\rightarrow\alpha$ structural transformation, which involves the moving of O atoms with Mo–O bond formation and destruction (described by arrows and slashes in Fig. 2(top-right)). The structural change in the molybdate groups can also be described as follows.

$$2\{Mo_4O_{15}\} + 2\{Mo_7O_{26}\} + 2\{MoO_4\} \rightarrow 3\{Mo_6O_{22}\} + 6\{MoO_4\}\ (\beta\rightarrow\alpha).$$

In conclusion, the $\beta\leftrightarrow\alpha$ transformation is achieved by partial rearrangement of O atoms, while the positions of La and Mo centers are almost retained. This result let us recall the flexibility of coordination numbers and geometries of the $\{RO_n\}$ and $\{MoO_{n'}\}$ polyhedra commonly observed in many materials.

3.2. Structural description of $R_2Mo_4O_{15}$ (R=Nd, Sm)

$R_2Mo_4O_{15}$ (R = Nd, Sm) is isomorphous with the R = Eu and Gd analogs [15], consisting of $R_3Mo_6O_{22.5}$ asymmetric unit (Table 2). The structure consists of one $\{Mo(6)O_5\}$ trigonal bipyramid, one $\{Mo(4)O_6\}$ octahedron, four $\{Mo(1,2,3,5)O_4\}$ tetrahedra, and three $\{R(1–3)O_8\}$ square-antiprisms. In the $\{Mo(4)O_6\}$ octahedron, Mo(4) is displaced from the center to the O(15)···O(17) edge as shown by the shorter Mo(4)–O(15) and –O(17) lengths (1.698(5)–1.719(4) Å) than others (1.8621(4)–2.198(4) Å). The $\{Mo(4)O_6\}$ and symmetry-related $\{Mo(4')O_6\}$ octahedra share the O(9) atom with a linear Mo(4)–O(9)–Mo(4′) linkage, forming a $\{Mo(4)_2O_{11}\}$ group. The $\{Mo(6)O_5\}$ polyhedron is composed of a $\{Mo(6)O_4\}$ tetrahedron with short Mo–O distances (1.735(5)–1.839(4) Å) and capped by O(18′) with a longer (2.291(5)–2.345(4) Å) distance. This geometry can also be viewed as a square pyramid (square of [O(18), O(18′), O(22), O(23)] and apical O(2)). $\{Mo(6)O_5\}$ is connected to $\{Mo(6')O_5\}$ via O(18) and O(18′) atoms to form a $\{Mo(6)_2O_8\}$ group. These $\{Mo(4)_2O_{11}\}$ and $\{Mo(6)_2O_8\}$ groups are linked alternately via O(22), giving rise to a corrugated $\{Mo_4O_{17}\}_\infty$ chain running along the a-axis (Fig. 3b). The $\{Mo(1,2)O_4\}$ tetrahedra are attached to the molybdate chain at O(11) and O(15) respectively (not shown in Fig. 3b), while $\{Mo(3,5)O_4\}$ are isolated from other molybdate polyhedra. The square-antiprismatic $\{R(1–3)O_8\}$ are dimerized as follows: $\{R(2)O_8\}$ and $\{R(3)O_8\}$ share the trigonal plane defined by O(7), O(21), and O(23) atoms, while $\{R(1)O_8\}$ and symmetry-related $\{R(1')O_8\}$ share the square-forming O(4), O(4′), O(5), and O(5′) atoms. The resulting $\{R_2O_{13}\}$ and $\{R_2O_{12}\}$ groups are isolated. The former $\{R_2O_{13}\}$ group is often observed in other rare earth molybdates, such as $R_2Mo_4O_{15}$ (R = La [9], Ce [10], Pr [11]), $R_4Mo_7O_{27}$ and $R_6Mo_{10}O_{39}$ (R = Eu and Gd) [16]. The latter

$\{R_2O_{12}\}$ group, where the two R centers are quadruply linked by O atoms, is unusual in R molybdates. A similar $\{R_2O_{12}\}$ group has been found in $Nd_4Ni_3O_8$ [27], although the $\{NdO_8\}$ moiety has a cubic coordination. The R center in $\{R(1)O_8\}$ is shifted towards the [O(1), O(2), O(3), O(6)] plane due to the electrostatic repulsion acting between the $R(1)$ and $R(1')$ centers.

Replacement of R with Nd, Sm, Eu, and Gd gives rise to a small change in the $R_2Mo_4O_{15}$ structure. An increase in ionic radius (r) of R^{3+} [8] from Gd (1.053 Å) to Nd (1.109 Å) lengthens the R–O bonds by ca. 0.05 Å. This effect reflects directly an elongation of $R\cdots R$ distances as shown in Fig. 4a, where both $R1\cdots R1$ and $R2\cdots R3$ distances increased linearly with increasing r. The lengthening of the R–O bonds also causes an overall expansion of the unit cell: lengths of the a-, b-, and c-axes increase by 1.7%, 1.2%, and 1.1%, respectively, from R = Gd to Nd. Since the molybdate $\{Mo_4O_{17}\}_\infty$ chain lies parallel to the a-axis, the lattice expansion should also stretch the molybdate chain by 1.7%. Fig. 4b and c represent plots of the Mo–O distances within the $\{Mo(4)O_6\}$ and $\{Mo(6)O_5\}$ polyhedra (which form the molybdate chain) against r, respectively. One may notice that the Mo(6)–O(18′) length increases by 3.9% from R = Gd to Nd, while other Mo–O bonds exhibit no observable change. It seems reasonable that the longest (viz. the loosest) Mo(6)–O(18′) bond is predominantly affected by an external distortion. Therefore, we conclude that the ionic size of R^{3+} in $R_2Mo_4O_{15}$ affects only the longest Mo–O bond in the polymeric $\{Mo_4O_{17}\}_\infty$ groups.

3.3. Structural comparison in the $R_2Mo_4O_{15}$ family

As a result of this study, the $R_2Mo_4O_{15}$ family is categorized into five structures, I: R = La (α-form) [10], I′: R = La (β-form in this study), II: R = Ce [11] and Pr [12], III: R = Nd–Gd, and IV: R = Tb [13] and Ho [14]. Reviewing the large diversity of the R–O and Mo–O coordination patterns in the I–IV structures, it seems difficult to discover structural similarity among them. For example, structures of the molybdate groups appear to be completely different in I, II, III, and IV, which contain $\{Mo_6O_{22}\}$, $\{Mo_4O_{14}\}_\infty$, $\{Mo_4O_{17}\}_\infty$, and $\{Mo_4O_{15}\}$ groups, respectively [10–14]. Although I, II, and III have similar dimeric $\{R_2O_{13}\}$ groups with short $R\cdots R$ separations, IV does not. Fig. 5a–d represents arrangements of only R and Mo atoms in I–IV, respectively. Structure I′ is omitted because the metallic arrangement is practically the same as I. One can find a common cationic structure in Fig. 5a–d: R–R pair surrounded by 12 Mo atoms which is denoted by a $\{R_2Mo_{12}\}$ unit hereafter. In the top selections in Figs. 5a–d, the connections of R–Mo (with distances <6 Å) and R–R (in the $\{R_2O_n\}$ dimers) are drawn by solid lines for only one $\{R_2Mo_{12}\}$ set, and the projection plane is selected so that it is approximately normal to the R–R direction. As the $\{RO_8\}$ groups are discrete in structure IV [13,14], the nearest two $\{RO_8\}$ groups was taken as the R–R pair. In the lattices of I–IV, the $\{R_2Mo_{12}\}$ units are connected with each other to form $\{R_2Mo_{12}\}_\infty$ chains, which are well-represented as their side views in the bottom selections of Fig. 5a–d.

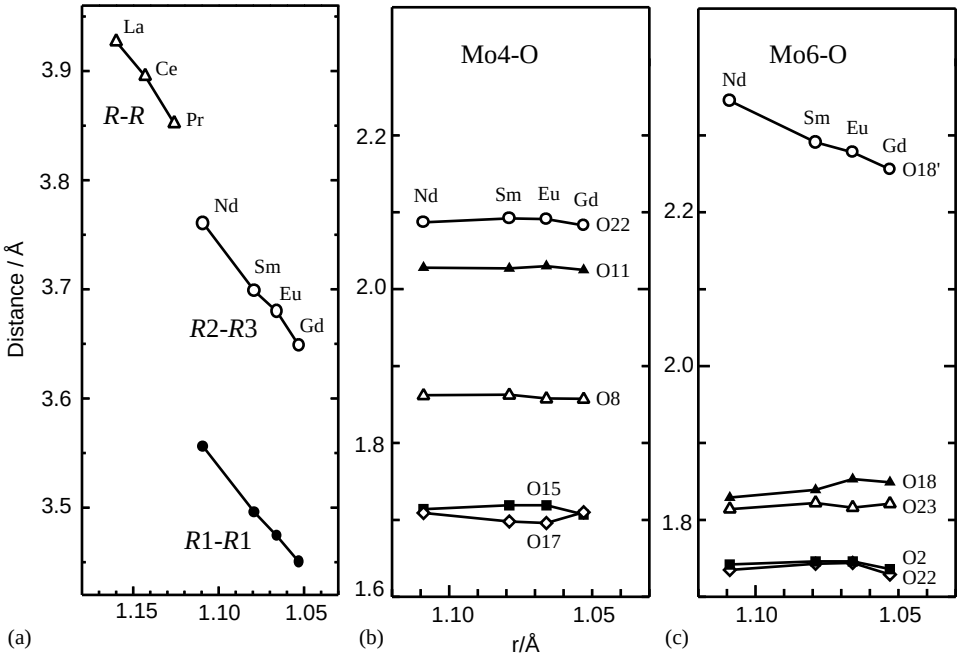

Fig. 4. Plots of the (a) $R\cdots R$, (b) Mo(4)–O, and (c) Mo(6)–O distances vs. ionic radius (r) of R^{3+} for $R_2Mo_4O_{15}$ (R = Nd, Sm, Eu, and Gd). The $R\cdots R$ distances for $R_6Mo_4O_{15}$ (R = La, Ce, and Pr) are also plotted with triangles in (a).

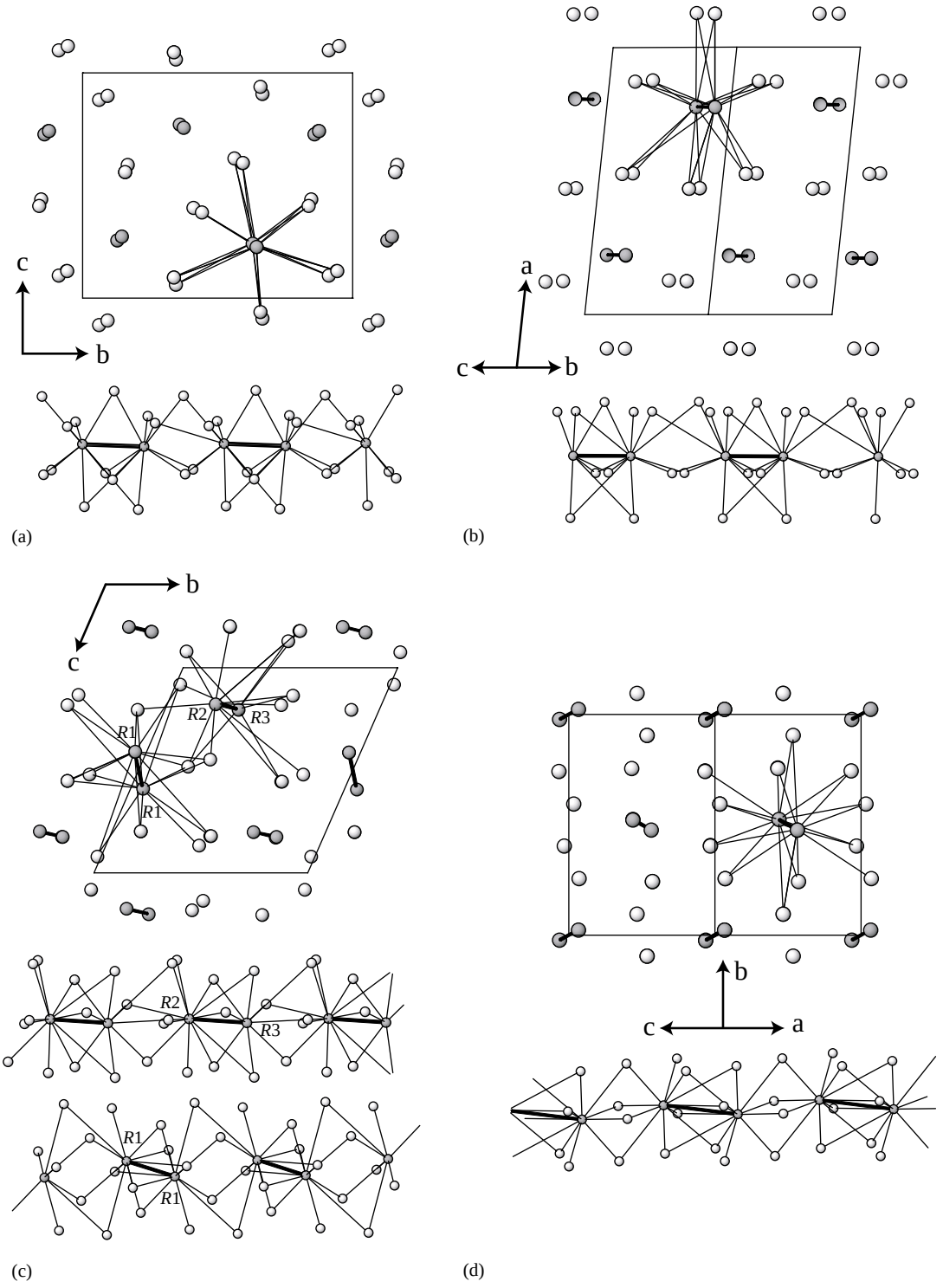

Fig. 5. Cationic arrangements in structures (a) I, (b) II, (c) III, and (d) IV. The dark- and light-gray spheres are R and Mo atoms, respectively. Within each $\{R_2Mo_{12}\}$ unit, connections between R and Mo (<6 Å) atoms, and within a R pair with the shortest R–R distances are drawn by the thin and thick solid lines, respectively. The side views of the $\{R_2Mo_{12}\}_\infty$ chains are represented in bottoms of (a)–(d).

Structure I exhibits the simplest arrangement (Fig. 5a top): in the $\{R_2Mo_{12}\}$ unit, a set of one R and hexagon-forming six Mo atoms ($\{RMo_6\}$ subunit) is almost superimposed on another $\{RMo_6\}$ subunit. This fundamental arrangement is maintained in structure II (Fig. 5b), although Mo atoms are substantially displaced and the R–R direction is slightly tilted with respect to the chain direction. Significant changes occur in III and IV (Fig. 5c and d), where positions of the 12 Mo atoms are much perturbed compared with I and II,

forming no longer Mo_6-hexagons. In addition, the tilting of the R–R directions is much enhanced, resulting in a zigzag conformation of the $\cdots R$–$R\cdots R$–$R\cdots$ framework in the $\{R_2Mo_{12}\}_\infty$ chain. There are two kinds of $\{R_2Mo_{12}\}$ units in structure III, one contains $R1$–$R1$ and the other $R2$–$R3$. Despite these relatively large transformations from I–II to III–IV, the topology of the R–Mo framework is retained. As shown in Fig. 4a, the R–R distance decreases in the sequence of I, II, and III, and increases immediately to $\sim$5.27 Å for IV (not plotted in Fig. 4a) where the $\{RO_8\}$ group is isolated. The isolation of the $\{RO_8\}$ group from III to IV by the replacement of Gd with Tb may be related to a large electrostatic repulsion between Tb atoms, i.e., a hypothetical $Tb_2Mo_4O_{15}$ compound with structure III would be more unstable than $Gd_2Mo_4O_{15}$ because of the shorter Tb–Tb distances (Tb1–Tb1: 3.4246 Å and Tb2–Tb3: 3.6245 Å estimated by linear extrapolations of the plots in Fig. 4a) than the Gd–Gd distances (3.4502(6) and 3.6484(4) Å, respectively [15]). In other words, the $R_2Mo_4O_{15}$ phase possessing R^{3+} with the size smaller than Gd^{3+} prefers structure IV to avoid the repulsion between the R atoms. It should be noted that no Tb(III) molybdate with Tb$\cdots$Tb distance shorter than 3.623 Å (which was observed in Tb_2MoO_6 [13]) is known.

References

[1] K. Aizu, A. Kumada, H. Yumoto, S. Ashida, J. Phys. Soc. Japan 27 (1969) 511.
[2] H.J. Borchardt, P.E. Bierstedt, Appl. Phys. Lett. 8 (1966) 50–52.
[3] G. Blasse, A. Bril, J. Chem. Pys. 45 (1966) 2350–2355.
[4] J. Huang, J. Lories, P. Porcher, J. Solid State. Chem. 43 (1982) 87–96.
[5] M. Ouwerkerk, F. Kellendonk, G. Blasse, J. Chem. Soc. Faraday Trans. 2 (78) (1982) 603–611.
[6] P. Lacorre, F. Goutenoire, O. Bohnke, R. Retoux, Y. Laligant, Nature 404 (2000) 856–858.
[7] F. Goutenoire, O. Isnard, R. Retoux, P. Lacorre, Chem. Mater. 12 (2000) 2575–2580.
[8] R.D. Shannon, Acta Crystallogr. A 32 (1976) 751–767.
[9] J.S. Xue, M.R. Antonio, L. Soderholm, Chem. Mater. 7 (1995) 333–340.
[10] F. Dubois, F. Goutenoire, Y. Laligant, E. Suard, P. Lacorre, J. Solid State Chem. 159 (2001) 228–233.
[11] G.D. Fallon, B.M. Gatehouse, J. Solid State Chem. 44 (1982) 156–161.
[12] V.A. Efremov, N.N. Davydova, V.K. Trunov, Russ. J. Inorg. Chem. 33 (1988) 1729–1732.
[13] H. Naruke, T. Yamase, Acta. Crystallogr. E 57 (2001) i106–i108.
[14] V.A. Efremov, N.N. Davydova, L.Z. Gokhman, A.A. Evdokimov, V.K. Trunov, Russ. J. Inorg. Chem. 33 (1988) 1732–1735.
[15] H. Naruke, T. Yamase, Inorg. Chem. 41 (2002) 6514–6520.
[16] H. Naruke, T. Yamase, J. Solid. State. Chem. 161 (2001) 85–92.
[17] H. Naruke, T. Yamase, Acta Crystallogr. E58 (2002) i62–i64.
[18] M.V. Mokohosoev, E.I. Get'man, Inorg. Mater. 5 (1969) 772–776.
[19] E.Y. Rode, G.V. Lysanova, L.Z. Gokhman, Inorg. Mater. 7 (1971) 1875–1877.
[20] T. Yamase, H. Naruke, J. Chem. Soc. Dalton Trans. (1991) 285–292.
[21] A. Altomare, M.C. Burla, M. Camalli, M. Cascarano, C. Giacovazzo, A. Guagliardi, G. Polidori, J. Appl. Crystallogr. 27 (1994) 435.
[22] W.H. Zachariasen, Acta. Crystallogr. 23 (1967) 558–564.
[23] T. Higashi, SHAPE—Program to obtain Crystal Shape using CCD camera, RigakuCorporation, Tokyo, Japan, 1999.
[24] T. Higashi, NUMABS—Numerical Absorption Correction, Rigaku Corporation, Tokyo, Japan, 1999.
[25] Rigaku Corporation and Rigaku/MSC, Crystal Structure Ver. 3.00, Tokyo, Japan.
[26] Molecular Structure Corporation, teXsan, Single Crystal X-ray Crystallographic Analysis Software, MSC, 3200 Research Forest Drive, The Woodlands, TX 77381, USA.
[27] R. Retoux, J. Rodriguez-Carvajal, P. Lacorre, J. Solid State Chem. 140 (1998) 307–315.